Supporting Information

Uranyl-based Metal-Organic Framework Featuring an Eight-connected U_4L_2 Cage for Guest Capture

Shuang Deng, [a, b] *Zhi-Wei Huang,* [b] *Xuan Fu,* [b] *Zhi-Heng Zhou,* [b] *Zhi-Ren Guo,* [b] *Lei Mei,* [b] *Ji-Pan Yu,* [b] *Yan-Qiu Zhu,* [a] *Nan-Nan Wang,* [*, a] *Kong-Qiu Hu,* [*, b] *Wei-Qun Shi* [*, b, c]

[a] State Key Laboratory of Featured Metal Materials and Life-cycle Safety for Composite Structures, School of Resources, Environment and Materials, Guangxi University, Nanning, 530004, Guangxi, China.

[b] Laboratory of Nuclear Energy Chemistry, Institute of High Energy Physics, Chinese Academy of Sciences, Beijing 100049, China.

[c] School of Nuclear Science and Engineering, Shanghai Jiao Tong University, Shanghai 200240, China.

Table of Contents

S1. Supplementary Methods

S2. Supplementary Figures

S3. Supplementary Tables

Table S5. Results of Langmuir, Freundlich and Themkin adsorption isotherm model fit to IHEP-50 organic dyes adsorption isotherms.

Table S6. Kinetic model parameters of IHEP-50 adsorption of gaseous iodine .

Table S7. Adsorption capacity of different iodine adsorbents.

S4. Supplementary References

S1. Supplementary Methods

Experimental Materials

Following reagents and chemicals were purchased from commercial sources and used without further purification. $UO_2(NO_3)_2 \cdot 6H_2O$ (99%, Institute of High Energy Physics, Chinese Academy of Sciences, Beijing), 4-formylbenzoic acid (98%, Energy Chemical), 4-(aminomethyl)benzoic acid (98%, Bidepharm), Sodium cyanoborohydride (98.4%, Bidepharm), concentrated HNO_3 (65.0~68.0%, Sinopharm Chemical Reagent Co., Ltd), sodium hydroxide (99%, Innochem), sodium bicarbonate (99%, 3AChem), N,N'-Dimethylformamide (DMF, 99%, Adamas). Caution! The uranyl nitrate ($UO_2(NO_{3)2} \cdot 6H_2O$) is a radioactive and chemically toxic reactant, precautions with suitable care and protection for handling such substances should be followed although it was used in the experiment.

Experimental Instruments

Nuclear magnetic resonance (NMR) spectra were obtained using a Bruker Avance III 500 MHz spectrometer (Bruker Inc., Switzerland) for determining the purity of the organic ligands, with deuterated dimethyl sulfoxide as the internal solvent resonance reference. Single crystal X-ray data of IHEP-50 were collected on a Bruker APEXII X-ray diffractometer equipped with a CMOS PHOTON 100 detector with a Mo-Kα X-ray source (Kα=0.71073 Å) or a Cu-Kα X-ray source (Kα = 1.54178 Å). The large structure of IHEP-50 is tricky to get good quality, high resolution data (1.0 for IHEP-50) from and the data resolution is lower than ideal. However, the structure is suitable to confirm connectivity. The SQUEEZE routine of PLATON was used to remove the diffraction contribution from disordered solvents (DMF) and counter ions $[(CH_3)_2NH_2]^+$ of IHEP-50. Powder X-ray diffraction measurements were made using a Bruker D8 Advance diffractometer with Cu Kα radiation (λ=1.5406 Å) in the range 3-50° (step size: 0.02°). IR measurements were obtained on a Bruker Tensor 27 infrared spectrometer. Sample was diluted with spectroscopic KBr and pressed into a pellet. The measured wavenumber is between 400 and 4000 cm^{-1}. Thermogravimetric analysis (TGA) was performed on a TA Q500 analyzer over the temperature range of 30-600 °C in an air atmosphere with a heating rate of 5 $°C \cdot min^{-1}$. The UV absorption spectra of organic dye solution were determined using a Hitachi U-3000 UV-Vis-NIR spectrometer. The FL spectra of the samples were collected and processed on the Edinburgh Fluorescence Spectrometer FLS1000.

Synthetic procedures

Synthesis of the new ligand H_6DTPCA was synthesized by following the route as shown in Scheme S1.[1-5] All the intermediates were characterized by ^{1}H NMR.

Synthesis of (E)- 4-((4-carboxybenzyl)imino)methyl)benzoic acid: 4-formylbenzoic acid (20.2 mmol) and 4-(aminomethyl)benzoic acid (21.5 mmol) were added in 350 mL of methanol solution, stirred at room temperature for 14 h, then filtered and washed with methanol (3×15 mL) and dried in an oven at 60 °C to obtain the white compound 1 ((E)- 4-((4-carboxybenzyl)imino)methyl)benzoic acid). (Yield: 92.6%). ^{1}H NMR (500 MHz, DMSO-d_6.) δ = 8.62 (s, 1H), 8.03 (d, J = 8.3 Hz, 2H), 7.94 (dd, J = 13.4, 8.3 Hz, 4H), 7.48 (d, J = 8.2 Hz, 2H), 4.89 (s, 2H).

Synthesis of 4,4′-(azenediylbis(methylene))dibenzoic acid: 28.8 mmol of sodium cyanoborohydride and compound 1 (17.3 mmol) were added to an anhydrous methanol suspension (100 mL) under ice bath conditions, stirred for 20 h, filtered and washed with methanol (3×15 mL), and then dried in an oven at 60 °C to obtain white compound 2 (4,4′-(azenediylbis(methylene))dibenzoic acid). (Yield: 73.0%). ^{1}H NMR (500 MHz, DMSO-d_6.) δ = 7.90 (d, J = 8.2 Hz, 4H), 7.47 (d, J = 8.2 Hz, 4H), 3.75 (s, 4H).

Synthesis of 4,4',4'',4''',4'''',4'''''-(((1,3,5-triazine-2,4,6-triyl)tris (azanetriyl)) hexakis(methylene))hexabenzoic acid (H_6DTPCA): compound 2 (9 mmol) was added to 20 mL distilled water under ice bath condition, then NaOH (20 mmol, 800 mg), $NaHCO_3$ (800 mg), and a solution of cyanuric chloride (3 mmol) in 6 mL 1, 4-dioxahexacyclic were added to the above suspension, stirred for 6 h, then stirred at room temperature for 12 h, and finally at 110 °C, reflux for 24 h. After the reaction, the solution was adjusted to pH=2 with 2 M hydrochloric acid, filtered and washed with water (3×25 mL), dried in an oven at 60°C to obtain the ligand H_6DTPCA. (Yield: 53.7%). ^{1}H NMR (500 MHz, DMSO-d_6.) δ = 7.77 (m, 12H), 7.22 (m, 12H), 4.73 (d, J = 21.8 Hz, 12H).

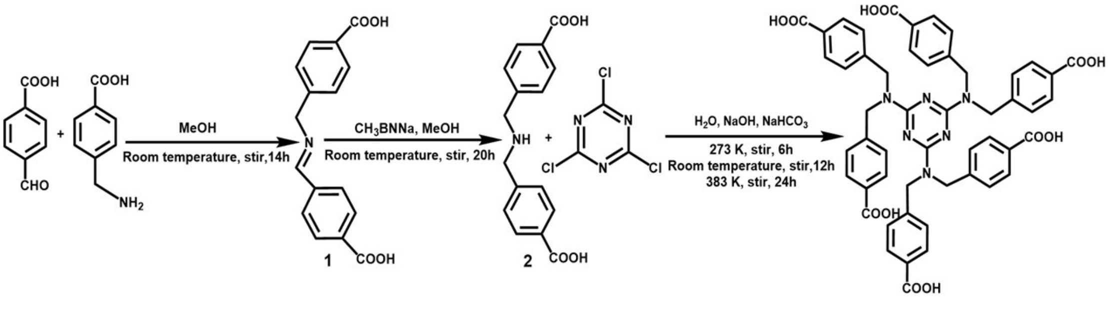

Scheme 1 Synthesis of H_6DTPCA ligand.

Experimental data fitting

Adsorption isothermal fitting was performed using Langmuir, Freundlich, and Temkin models with the following equations,[6] respectively:

Langmuir adsorption isotherm model: $C_e/Q_e = 1/(Q_m K_L) + C_e/Q_m$

Freundlich adsorption isotherm model: $ln(Q_e) = ln(K_f) + \frac{1}{n} ln(C_e)$

Temkin adsorption isotherm model: $Q_e = \frac{RT}{b} ln(C_e) + \frac{RT}{b} ln(K_m)$

where Q_e ($mg \cdot g^{-1}$) and C_e ($mg \cdot L^{-1}$) are the equilibrium adsorption capacity and adsorption concentration of organic dyes solution, respectively. Q_m ($mg \cdot g^{-1}$) is the theoretical maximum adsorption value, K_L ($L \cdot mg^{-1}$) and K_f ($(mg \cdot g^{-1})(L \cdot mg^{-1})^{1/n}$) are the adsorption constants for Langmuir and Freundlich adsorption isothermal models, respectively, and n is the Freundlich linear index. R ($J \cdot mol^{-1} \cdot K^{-1}$) is the universal gas constant, T (K) is the temperature, b ($J \cdot mol^{-1}$) is the Temkin constant related to the heat of sorption, and K_m ($L \cdot g^{-1}$) is the Temkin isotherm constant.

The kinetic equations for the pseudo-first-order and pseudo-second-order adsorption kinetic models are as follows:[7, 8]

Pseudo-first-order adsorption kinetic model: $Q_t = Q_e - Q_e \times e^{-K_1 t}$

Pseudo-second-order adsorption kinetic model: $t/Q_t = 1/(K_2 Q_e^2) + t/Q_e$

where K_1 (h^{-1}) and K_2 ($g \cdot mg^{-1} \cdot h^{-1}$) are pseudo-first-order and pseudo-second-order rate constants, respectively, and Q_t ($mg \cdot g^{-1}$) and Q_e ($mg \cdot g^{-1}$) are the amounts of organic dyes adsorbed per gram of sample at time t and at equilibrium, respectively.

S2. Supplementary Figures

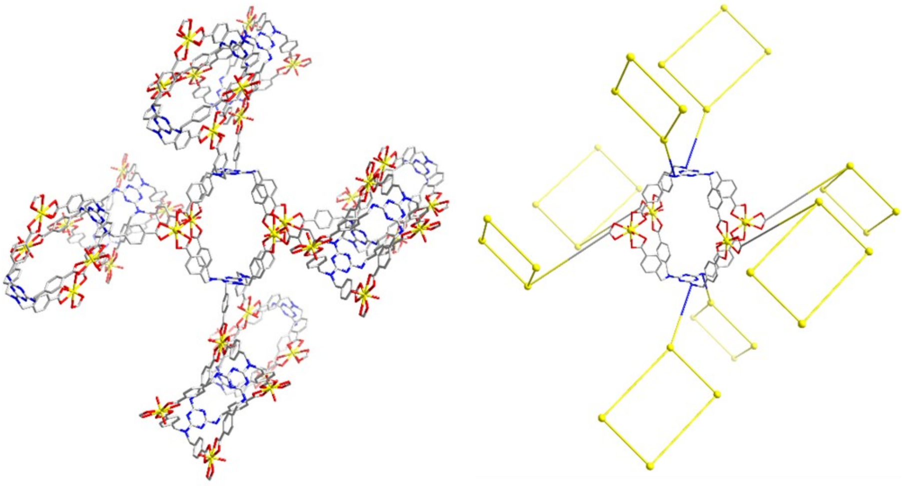

Figure S1. Connection model between U_4L_2 cages. Color scheme: U, yellow; C, gray;

O, red; N, blue. Hydrogen atoms were omitted for clarity.

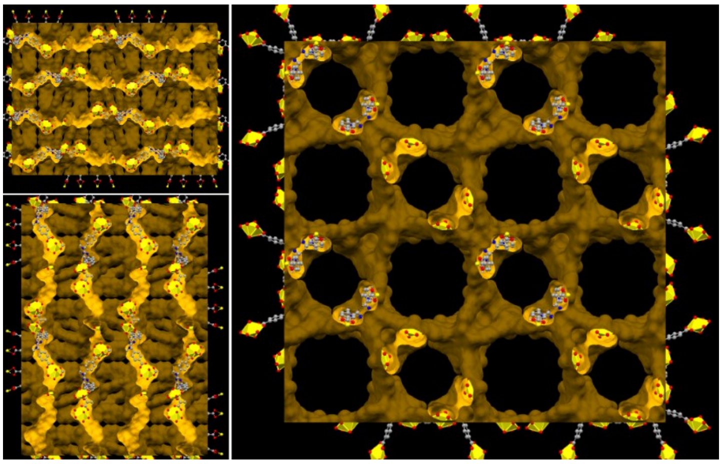

Figure S2. The 3D porous framework structure of IHEP-50 contains two types of 1D channels.

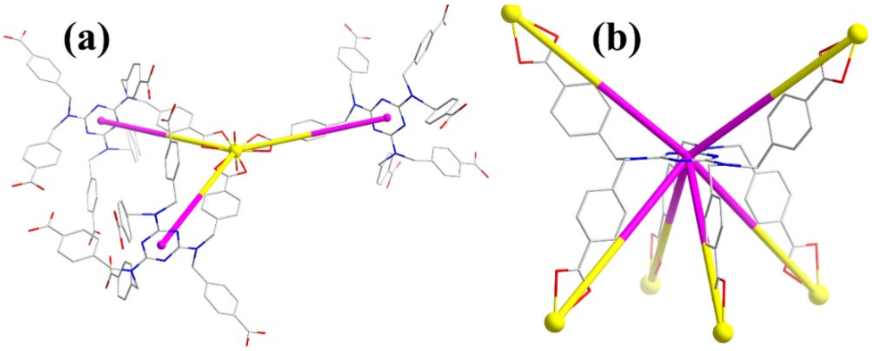

Figure S3. (a) The $UO_2(COO)_3^-$ unit viewed as a 3-connected node. (b) The $DTPCA^{6-}$ ligand viewed as a 6-connected node.

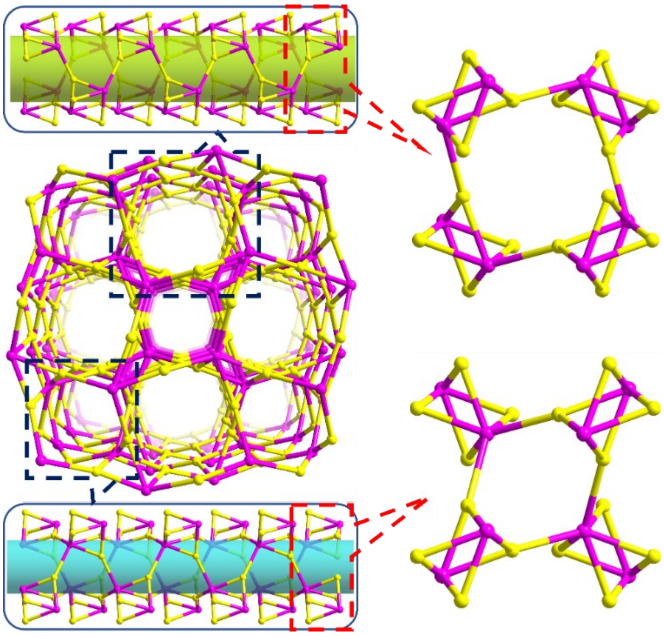

Figure S4. The U_4 octahedral cages are interconnected to form two different-sized 1D channel structures of IHEP-50.

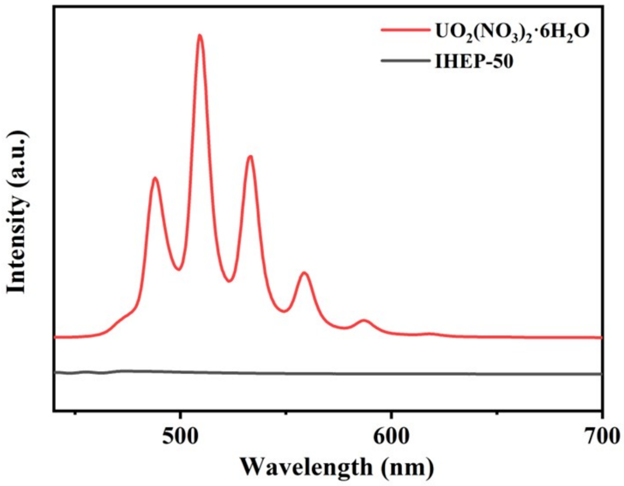

Figure S5. FL spectra of $UO_2(NO_3)_2\cdot 6H_2O$ and IHEP-50 (λ_{ex} = 375 nm).

Fluorescence spectra (Figure S1) showed that compared with the fluorescence intensity of uranyl nitrate, it can be found that uranyl ion has fluorescence quenching after binding with ligand to form crystal.

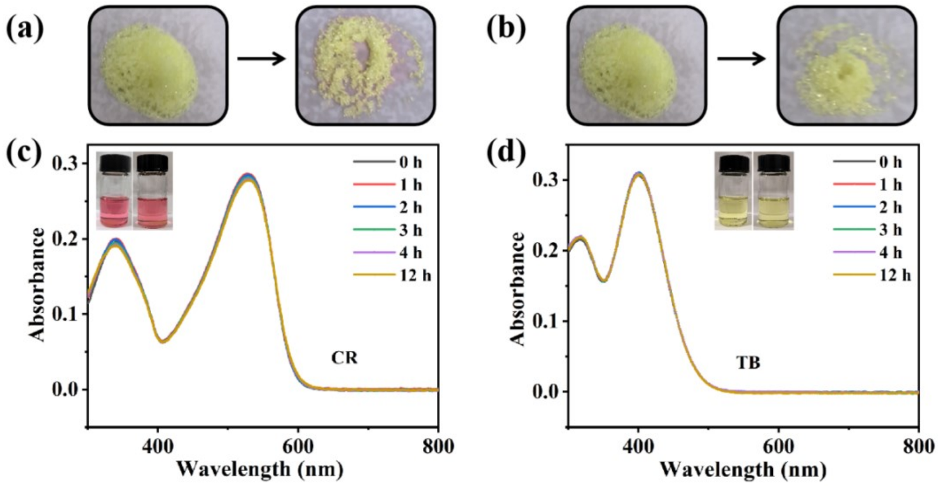

Figure S6. Color changes of IHEP-50 before and after adsorption of (a) CR and (b) TB dye molecules, UV-vis spectra of DMF solutions of (c) CR and (d) TB dye molecules in the presence of IHEP-50 at different times.

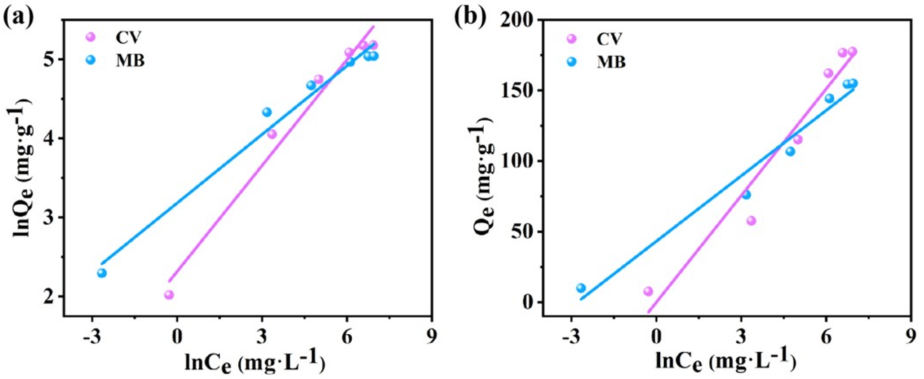

Figure S7. The adsorption isotherm results of IHEP-50 were fitted by (a) Freundlich and (b) Temkin model.

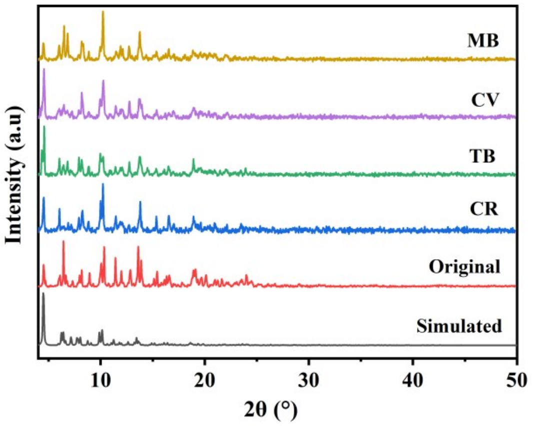

Figure S8. XRD patterns of IHEP-50 after adsorption in different dye solutions.

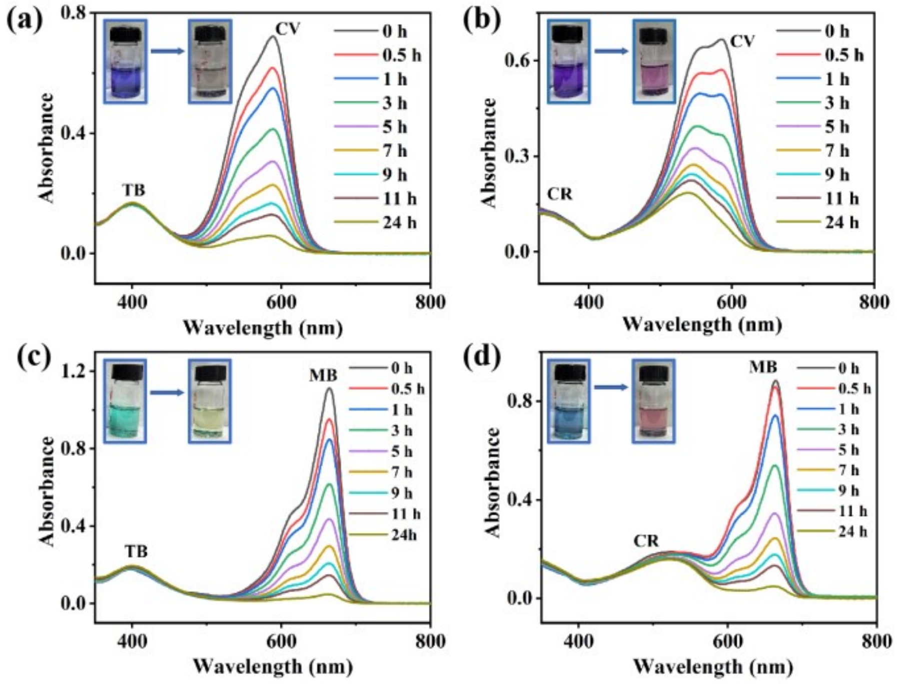

Figure S9. UV-Vis spectra of DMF solutions of 10 mg·g^{-1} mixed dyes (a) CV+TB, (b) CV+CR, (c) MB+TB, (d) MB+CR in the presence of IHEP-50 at different time.

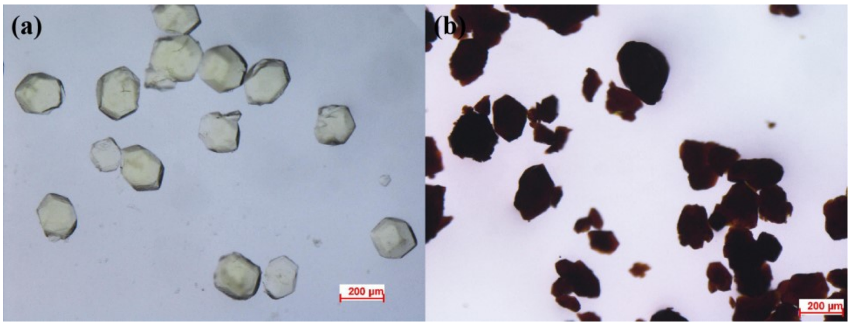

Figure S10. Micrographs of IHEP-50 before and after iodine adsorption in iodine/cyclohexane solution.

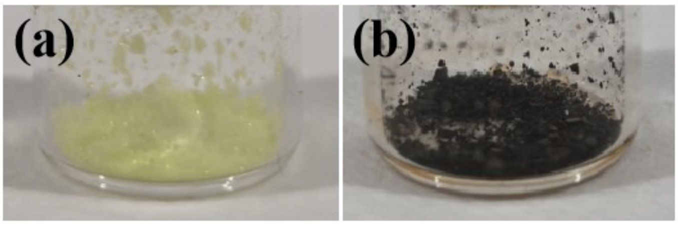

Figure S11. IHEP-50 crystals before and after gaseous iodine adsorption.

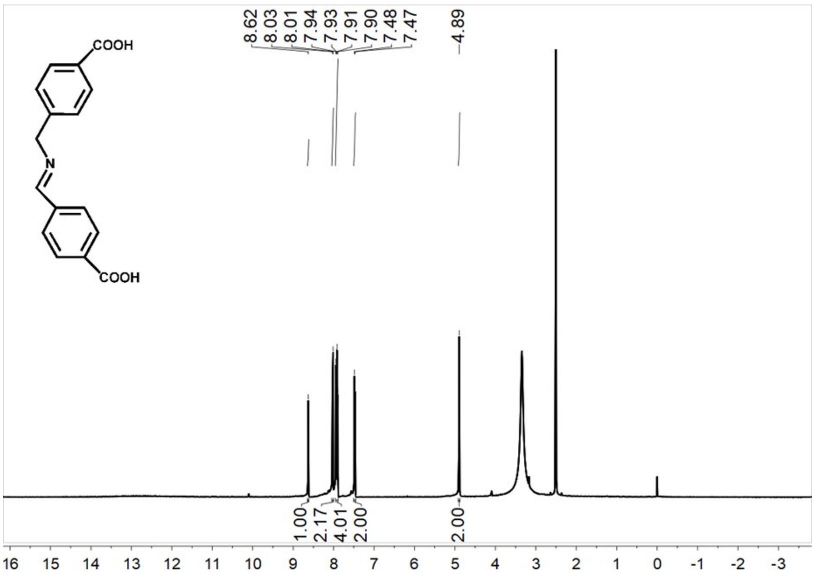

Figure S12. ^{1}H NMR spectrum of 1.

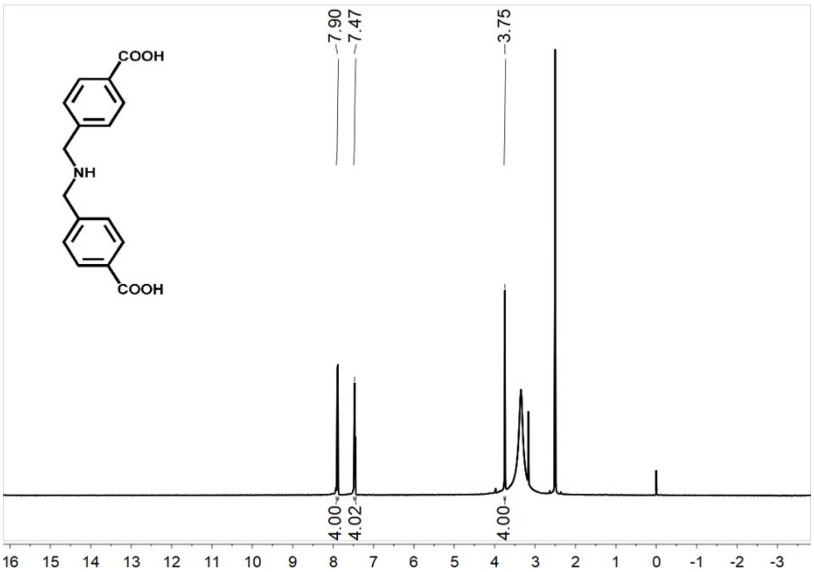

Figure S13. ^{1}H NMR spectrum of 2.

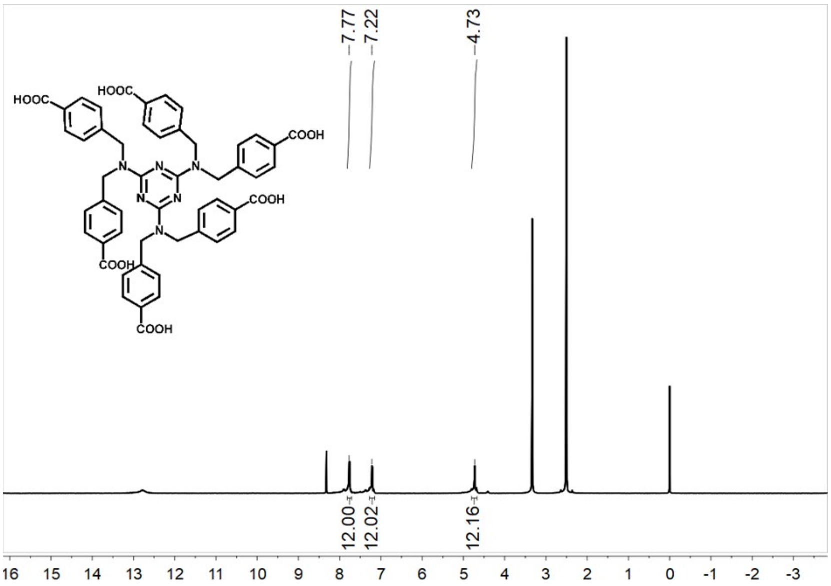

Figure S14. ^{1}H NMR spectrum of H_6DTPCA.

S3. Supplementary Tables

Table S1. Crystallographic data and structural refinement details of IHEP-50.

Compound	**IHEP-50**
Molecular formula	$C_{165}H_{302}N_{44}O_{54}U_2$
Fw	4242.55
T / K	170 K
CCDC No.	2411832
Radiation	1.54178
Crystal system	Tetragonal

Space group	$P4_2/ncm$
a (Å)	39.072 (2)
b (Å)	39.072 (2)
c (Å)	28.851 (3)
α(deg)	90
β(deg)	90
γ (deg)	90
V (Å^3)	44045 (6)
Z	8
ρ (calc) (g /cm^3)	1.280
F (000)	17728
Absorp.coeff. (mm^{-1})	4.778
θ range (deg)	1.599 to 50.511
Reflns collected	205417 (R_{int} = 0.0955)
Indep. reflns	11860
Refns obs. [$I > 2\sigma(I)$]	7008
GOF	1.086
$^{a}R_1$ /$^{b}wR_2$ [$I > 2\sigma(I)$]	0.0764 /0.2262
$^{a}R_1$ /$^{b}wR_2$ (all data)	0.1099 /0.2617

Table S2. Selected bond distances (Å) of IHEP-50.

Atom	**Bond Distances (Å)**	**Atom**	**Bond Distances (Å)**
U1-O1	1.773(8)	N4-C25	1.548(15)
U1-O2	1.657(7)	O6-C7	1.308(13)
U1-O5	2.426(10)	O5-C7	1.293(14)
U1-O6	2.474(8)	C8-C7	1.458(17)
U1-C7	2.872(14)	C8-C9	1.394(17)
N1-C14	1.629(17)	C8-C13	1.367(16)
N1-C22	1.676(17)	O8-C21	1.299(11)
N1-C23	1.338(13)	O7-C21	1.243(11)
C1-C26	1.472(15)	C9-C10	1.464(19)
C1-O3	1.310(14)	C10-C11	1.389(19)
C1-O4	1.263(14)	C11-C12	1.350(17)
N2-C23	1.349(12)	C11-C22	1.505(18)
N2-C24	1.363(9)	C12-C13	1.437(16)
C2-C3	1.390(0)	C15-C19	1.390(0)
C2-C26	1.390(0)	C15-C20	1.390(0)
C3-C4	1.390(0)	C15-C14	1.526(14)
C4-C6	1.390(0)	C19-C18	1.390(0)
C4-C25	1.576(14)	C18-C17	1.390(0)
C6-C5	1.390(0)	C17-C16	1.390(0)
C5-C26	1.390(0)	C17-C21	1.488(12)
N3-C23	1.351(12)	C16-C20	1.390(0)
N4-C24	1.346(18)		

Table S3. Selected angles (°) of IHEP-50.

Atom	**Angles (°)**	**Atom**	**Angles (°)**
O1-U1-O6	89.8(3)	O6-C7-C8	119.2(13)
O1-U1-O5	90.2(4)	O5-C7-O6	116.1(12)
O1-U1-C7	88.4(4)	O5-C7-C8	124.2(13)
O2-U1-O1	178.7(4)	C8-C9-C10	116.4(15)
O2-U1-O6	89.4(3)	C11-C10-C9	121.0(15)
O2-U1-O5	90.1(4)	C10-C11-C22	116.9(15)
O5-U1-O6	53.3(3)	C12-C11-C10	119.3(15)
C14-N1-C22	135.9(12)	C12-C11-C22	123.8(15)
C23-N1-C14	112.5(12)	C11-C12-C13	121.9(14)
C23-N1-C22	111.6(12)	C19-C15-C20	120.0(0)
O3-C1-C26	119.7(12)	C19-C15-C14	118.4(8)
O4-C1-C26	121.9(12)	C20-C15-C14	121.7(8)
O4-C1-O3	118.4(13)	C18-C19-C15	120.0(0)
C23-N2-C24	112.0(11)	C19-C18-C17	120.0(0)
C3-C2-C26	120.0(0)	C18-C17-C21	120.7(7)
C2-C3-C4	120.0(0)	C16-C17-C18	120.0(0)
C3-C4-C25	118.9(9)	C16-C17-C21	119.3(7)
C6-C4-C3	120.0(0)	C20-C16-C17	120.0(0)
C6-C4-C25	120.8(9)	C16-C20-C15	120.0(0)
C5-C6-C4	120.0(0)	C15-C14-N1	107.4(10)
C6-C5-C26	120.0(0)	C8-C13-C12	118.2(13)
C2-C26-C1	120.2(9)	O8-C21-C17	118.2(10)
C5-C26-C1	119.8(9)	O7-C21-O8	120.7(10)
C5-C26-C2	120.0(0)	O7-C21-C17	120.9(10)
C24-N4-C25	116.2(9)	C11-C22-N1	105.3(11)
C7-O6-U1	93.7(8)	N1-C23-N2	114.7(11)
C7-O5-U1	96.3(8)	N1-C23-N3	119.3(12)
C9-C8-C7	115.2(14)	N2-C23-N3	125.9(12)
C13-C8-C7	121.8(13)	N4-C24-N2	115.6(7)
C13-C8-C9	122.6(14)	N4-C25-C4	116.3(12)

Table S4. Pseudo-first order adsorption kinetic model and pseudo-second order adsorption kinetic model of IHEP-50 in organic dyes solution.

	Pseudo-first-order adsorption kinetics model			Pseudo-second-order adsorption kinetics model		
	Q_e (mg·g^{-1})	K_1 (h^{-1})	R^2	Q_e (mg·g^{-1})	K_2 (g·mg^{-1}·h^{-1})	R^2
CV	9.19	0.1672	0.9972	11.05	0.0147	0.9831
MB	11.60	0.1375	0.9973	14.64	0.0081	0.9625

Table S5. Results of Langmuir, Freundlich and Themkin adsorption isotherm model fit to IHEP-50 organic dyes adsorption isotherms.

Adsorption isothermal model	Parameter	CV	MB
Langmuir isotherm model	Q_m (mg·g^{-1})	187.62	158.73
	K_L (L·mg^{-1})	0.0174	0.0341
	R^2	0.9963	0.9982
Freundlich isotherm model	K_f (mg·g^{-1})(L·mg^{-1})$^{1/n}$	10.14	24.11
	n	2.2379	3.4559
	R^2	0.9751	0.9801
Temkin isotherm model	K_m (L·g^{-1})	0.9974	0.0611
	b	25.20	15.45
	R^2	0.9489	0.9677

Table S6. Kinetic model parameters of IHEP-50 adsorption of gaseous iodine .

	Pseudo-first-order adsorption kinetics model			Pseudo-second-order adsorption kinetics model		
	Q_e (mg·g^{-1})	K_1 (h^{-1})	R^2	Q_e (mg·g^{-1})	K_2 (g·mg^{-1}·h^{-1})	R^2
IHEP-50	253.98	0.7550	0.9920	303.95	0.0023	0.9816

Table S7. Adsorption capacity of different iodine adsorbents.

MOFs	Equilibration time (h)	Adsorption capacity (mg·g^{-1})	Ref.
IHEP-50	9	253.5	this work
SM-3	40	157.5	[9]
UiO-66-NH_2	48	527	[10]
12bX-AgI	24	330	[11]
Dy-UiO-66	200	150	[12]
Ag-attached silica gel	–	40.60 - 238.83	[13]
Lead-vanadate sorbents	16	155	[14]
3DOM-SiO_2	–	15.2±0.9	[15]
PAN	10	72.1	[16]
AgX	360	255	[17]

Zeolite	–	52.05 - 220.71	18
Ag^0Z	–	105±5	19

S4. Supplementary References

(1) P. de Hoog, P. Gamez, W. L. Driessen, J. Reedijk. *Tetrahedron Lett.* **2002,** 43 (38), 6783-6786.

(2) A. de Bettencourt-Dias, R. M. Beeler, J. R. Zimmerman. *J. Am. Chem. Soc.* **2019,** 141 (38), 15102-15110.

(3) A. de Bettencourt-Dias, R. M. Beeler, J. R. Zimmerman. *Inorg. Chem.* **2020,** 59 (1), 151-160.

(4) K. Lv, S. Fichter, M. Gu, J. März, M. Schmidt. *Coord. Chem. Rev.* **2021,** 446, 214011.

(5) M. H. Yu, X. T. Liu, B. Space, Z. Chang, X. H. Bu. *Coord. Chem. Rev.* **2021,** 427, 213518.

(6) S. Sağlam, F. N. Türk, H. Arslanoğlu. *J. Environ. Chem. Eng.* **2023,** 11 (5), 110568.

(7) Q. z. Wang, Y. j. Zhao, Z. Shi, X. Sun, T. Bu, C. q. Zhang, Z. x. Mao, X. Li, L. Wang. *Chem. Eng. J.* **2021,** 420, 129955.

(8) T. T. Li, Y. M. Liu, T. Wang, Y. L. Wu, Y. L. He, R. Yang, S. R. Zheng. *Microporous Mesoporous Mater.* **2018,** 272, 101-108.

(9) S. Kamal, M. Khalid, M. S. Khan, M. Shahid, M. Ahmad. *Dalton Trans.* **2023,** 52 (14), 4501-4516.

(10) A. Abramova, N. Couzon, M. Leloire, P. Nerisson, L. Cantrel, S. Royer, T. Loiseau, C. Volkringer, J. Dhainaut. *ACS Appl. Mater. Interfaces.* **2022,** 14 (8), 10669-10680.

(11) S. Chong, B. J. Riley, J. A. Peterson, M. J. Olszta, Z. J. Nelson. *ACS Appl. Mater. Interfaces.* **2020,** 12 (23), 26127-26136.

(12) C. Zwanziger, W. D. do Pim, A. A. Kitos, J. S. Ovens, P. J. Pallister, M. Murugesu. *Chem. Commun.* **2022,** 58 (91), 12700-12703.

(13) J. J. Wang, M. C. Li, Y. X. Feng, Y. Liu, J. T. Liu. *Nucl. Mater. Energy.* **2022,** 33.

(14) R. Pénélope, L. Campayo, M. Fournier, S. Le Gallet, A. Gossard, A. Grandjean. *Front. Chem.* **2022,** 10.

(15) S. Chang, K. J. Wang, X. M. Song, J. G. Liu, J. L. Chen, Z. Q. Zhang, Y. G. Li. *Prog. Nucl. Energy.* **2022,** 151.

(16) L. Zhang, M. F. Li, X. Liu, J. Q. Feng, Y. J. Liu, Y. Z. Tu, S. Y. Li, T. Duan. *Chem. Eng. J.* **2024,** 493.

(17) A. Yadav, S. H. Chong, B. J. Riley, J. S. McCloy, A. Goel. *Ind. Eng. Chem. Res.* **2023,** 62 (8), 3635-3646.

(18) S. L. Xu, J. J. Wang, Y. X. Feng, Y. Liu, J. T. Liu. *Nucl. Mater. Energy.* **2023,** 37.

(19) Z. H. Shen, A. I. Wiechert, A. P. Ladshaw, A. Greaney, C. Tsouris, S. Yiacoumi. *Chem. Eng. J.* **2024,** 482.